

Available online at [www.sciencedirect.com](http://www.sciencedirect.com)

**jmr&t**  
Journal of Materials Research and Technology  
journal homepage: [www.elsevier.com/locate/jmrt](http://www.elsevier.com/locate/jmrt)



## Original Article

# Reimann Brake Ramp for planar flow casting processes and analysis of ribbon gluing



Laurent Marot<sup>\*</sup>, Silvester Jakob, Marco Martina, Peter Reimann<sup>†</sup>,  
Heinz Breitenstein, Michael Steinacher, Ernst Meyer

Department of Physics, University of Basel, Klingelbergstrasse 82, 4056, Basel, Switzerland

## ARTICLE INFO

## Article history:

Received 10 June 2021

Accepted 24 November 2021

Available online 14 December 2021

## Keywords:

Planar flow casting  
Amorphous metallic glass  
Melt puddle  
Herringbone defect  
Ribbon gluing  
Cooling rate

## ABSTRACT

Planar flow casting is a rapid solidification process used to manufacture thin, metallic ribbons, and foil. Liquid metal is forced through a nozzle against a heat-sink wheel, and it rapidly solidifies into thin ribbons. A puddle of molten metal, held by surface tension, forms between the nozzle and wheel. This study examines a well-defined periodic surface defect called herringbone (HB), which is commonly produced when casting zirconium based alloys. The presence of this defect is related to processing conditions and puddle dynamics. Its formation has been correlated with the pinning of the liquid puddle at the nozzle edge. Here, the uniformity of thickness along a ribbon was successfully controlled (over a length of 50 m) using the Reimann Brake Ramp, which reduces the wheel speed at the start of the cast. For the alloy used in this study, the variation in the dimensionless thickness parameter,  $\tau/G$ , with the Euler number ( $Eu = \Delta P/\rho U^2$ ) at assigned values of  $B/G$  followed an allometric scaling, with an exponent value close to the theoretical value of  $1/3$ . Furthermore, the nozzle inclination was related to the ribbon thickness,  $\tau$ , and the ribbon quality. Moreover, a newly developed automatized melt spinner permitted monitoring and controlling of the process parameters, elucidating the gluing phenomenon of the ribbon observed during the starting phase. The ribbon gluing was influenced by the puddle geometry, the recirculation in the puddle, and later, to the ribbon cooling rate. Within these results, high-quality ribbons with control thickness over a considerable length are achieved.

© 2021 The Author(s). Published by Elsevier B.V. This is an open access article under the CC BY-NC-ND license (<http://creativecommons.org/licenses/by-nc-nd/4.0/>).

## 1. Introduction

Planar flow casting (PFC) is a rapid solidification technique for producing thin metal sheets and ribbons. Generally, ribbons

are used as brazing foils for joining metal or ceramic pieces [1] and other applications like catalysts for water splitting [2] or shape memory foils [3] and also for hydrogen storage [4]. Figure 1 shows a schematic representation of melt flow from the crucible, surrounded by a water-cooled induction heating

<sup>\*</sup> Corresponding author.

E-mail address: [laurent.marot@unibas.ch](mailto:laurent.marot@unibas.ch) (L. Marot).

<sup>†</sup> Deceased author.

<https://doi.org/10.1016/j.jmrt.2021.11.129>

2238-7854/© 2021 The Author(s). Published by Elsevier B.V. This is an open access article under the CC BY-NC-ND license (<http://creativecommons.org/licenses/by-nc-nd/4.0/>).

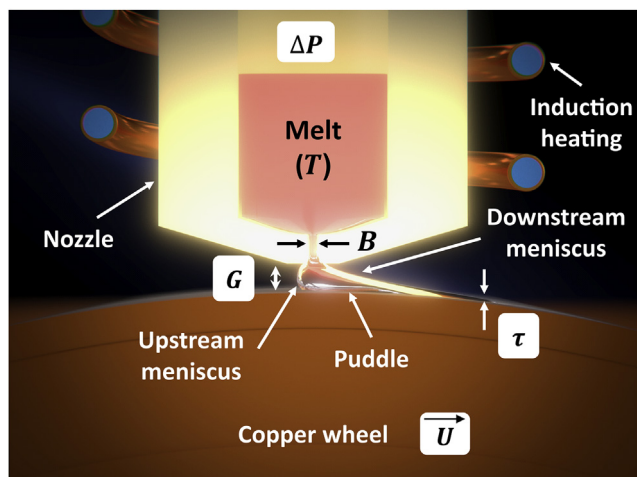


Fig. 1 – Side-view sketch of planar flow casting process.

coil, through a nozzle of breadth  $B$  onto a rotating metallic wheel (linear velocity,  $U$ ). This is achieved by applying inert gas pressure ( $\Delta P$ ). At the contact zone between the nozzle and the rotating wheel gap, named  $G$ , liquid metal forms an upstream meniscus (USM) and a downstream meniscus (DSM), which move throughout the entire cast and are constrained by surface tension; this is called a puddle. The water-cooled rotating copper wheel removes the heat underneath the puddle, enabling solidification. A thin layer of solidified material is dragged out of the puddle, leading to amorphous ribbon formation with a thickness of  $\tau$ .

The essential features of the PFC system were presented schematically by Phair et al. [5], who depicted all of the critical process parameters that must be regulated for the most efficient operation of the casting facility. The melt temperature,  $T$  (Fig. 1), the flow rate of the molten metal, the positioning of the casting nozzle, and the speed of the wheel are all key parameters influencing the production of high-quality strips. Moreover, as described by Sundararajan et al., all these parameters are linked [6].  $\Delta P$  and  $G$ , for example, have a direct influence on the flow rate, which is directly related to  $\tau$ .  $U$  and  $T$  are both inversely proportional to  $\tau$ . Moreover,  $G$  also changes with time due to the wheel heating up. Wheel

expansion reduces  $G$ , increasing the hydrodynamic resistance to flow, and hence reduces the flowrate for a constant applied pressure drop,  $\Delta P$ . Indeed, monitoring and controlling of the previously described parameters are the main challenges of the PFC process [7] and have a strong influence on the ribbon metallurgical properties [3,8].

In this work, we focus on a new method to control the ribbon thickness over a length of 50 m by reducing the wheel speed at the start of the cast. This method was not already reported and will be named using his inventor's name as Reimann Brake Ramp. Moreover, the development of an automatized melt spinner permitted monitoring and controlling the process parameters, elucidating the ribbon's gluing phenomenon during the starting phase.

## 2. Experimental

### 2.1. Melt spinner

The Department of Physics at the University of Basel has significant expertise in the fabrication and characterization of metallic glasses [9] and ribbons for active brazing foil. The co-existence of icosahedral and chain-like structures was recently demonstrated by Pawlak et al.; this might prove to be essential for understanding the mechanical properties of metallic glasses [10]. Production of ribbon metallic glasses was started at the end of the 1970s on the melt spinner (MS1) presented in Fig. 2. In 2017, this activity was advanced further with the construction of a new melt spinner (Fig. 2b) to improve capability; the new melt spinner features state-of-the-art sensors and controllers to optimize the melt spinning process. Casting is possible in the manual or automatic mode; in the latter case, a recipe is sent to the controller, and the process starts automatically. This mode substantially reduces the uncertainties associated with human error. Recently, a new method was developed in which the molten metal is ejected from the crucible without the need for an operator to monitor the temperature and manually release the ejection gas, this is termed Auto Ejection Melt Spinning (AEMS) [11].

The wheel (diameter of 300 mm) is produced from oxygen-free high-thermal-conductivity (OFHC) copper. Its width is 65 mm, and it has a typical oblong profile that extends a

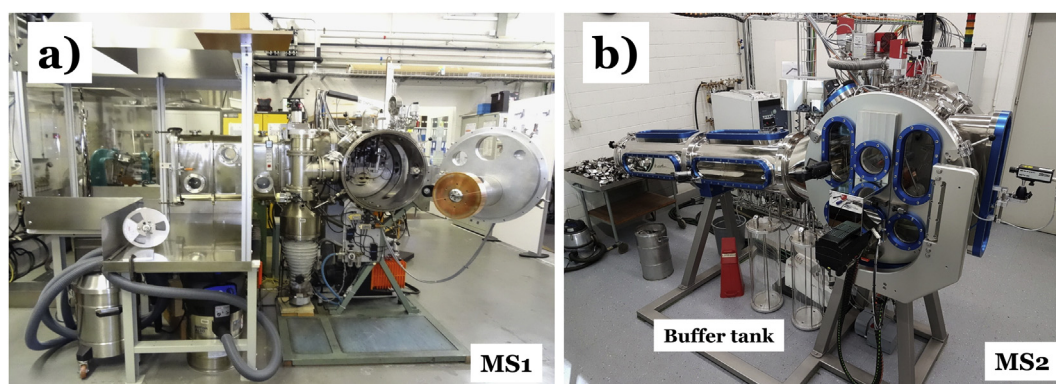


Fig. 2 – (a) Melt spinner 1 (MS1) and (b) Melt Spinner 2 (MS2).

maximum of 50  $\mu\text{m}$  along the width. For MS1 and MS2, the arithmetic average of the roughness profile is approximately 0.2  $\mu\text{m}$ . For MS2, the wheel has recently been equipped with water cooling; however, all results presented herein were obtained without water cooling for either MS. The gas inside the chamber, which is used to apply  $\Delta P$ , is air or an inert gas; typically, argon (Ar) or helium (He) to obtain a high cooling rate (He has ten times higher thermal conductivity as Ar at ambient condition [12]). For the purposed of this study, helium was used. For typical casts reported herein, a rectangular slot of breadth  $B = 0.5 \text{ mm}$  and width  $W = 35 \text{ mm}$  was machined into the graphite nozzle. The chamber was first pumped until a vacuum pressure of  $10^{-3} \text{ Pa}$  was reached, before being filled with helium at atmospheric pressure during casting. A zirconium based alloyed was used in this study.

## 2.2. Reimann Brake Ramp

As seen in Fig. 1, an inert gas pressurizes the crucible in a manner that compensates for the decreasing hydrostatic pressure as the metal flows out (pressure-compensated PFC). Byrne et al. have predicted that if the argon pressure is set correctly, then the thickness of the ribbon may be either maintained at a constant value or increased on average [13]. However, at the largest length scales, on the order of 30 m, the ribbon is gradually thinned from beginning to end due to the gradual shrinking of the gap (on average). This offers increased hydrodynamic resistance to the flow and hence results in lower flow rates. This effect can be compensated for by increasing the pressure head by a preprogrammed amount [13]. At the start of MS1, the PC-PFC technique was not used; instead, the Reimann Brake Ramp (RBR)-PFC was implemented. The RBR provides a constant reduction in  $U$  at the start of the cast to compensate for the pressure decrease. The RBR was also used in the same manner for MS2. The effect of the RBR on the ribbon thickness is detailed in Section 3.2.

## 3. Results and discussion

### 3.1. Investigation of ribbon gluing

A recently developed process for MS2 is depicted in a video [14] showing the development of issues associated with the ribbon-gluing phenomenon that occurred during the initial phase of MS2. With parameters similar to those used for MS1, fatal gluing of the ribbons was observed for approximately 70% of the casts (Fig. 3). Glued ribbons are not useable as brazing foils. It is known that precise control of the melt temperature, the flow rate of the molten metal, the positioning of the casting nozzle, and the speed of the wheel are all

essential for the production of high-quality strips. At present, the PFC process, even if insufficiently understood, enables prediction of the optimum operating window for the production of uniform, high-quality ribbons in combination with the desired microstructure [5,15]. With the MS1 parameters applied to MS2, the process was already in the optimum operating window, as evidenced by the production of an amorphous ribbon (measured by X-Ray Diffraction) without herringbone (HB), cross wave, or striated patterns. However, the gluing phenomenon observed revealed that the interrelation between the various process parameters is complex and must be considered when optimizing the casting conditions [5]. Transients are always present and can be challenging to control. The stability of the flow configuration can significantly affect the likelihood of one or another puddle geometry being established and, perhaps, the occurrence of gluing. The stability of flow is also known to be closely related to the position, angle, and other parameters of the nozzle relative to the wheel. The various process parameters were investigated in detail to address this issue. The heat flux on the wheel varies dramatically; it has a peak value in the puddle region and then decreases rapidly in the circumferential direction [16]. The region of rapidly decreasing heat flux is mainly located in the first tens millimeters under the puddle [17]. As a result, for MS2, even a change in the length of the ribbon in contact with the copper wheel (called the sticking distance [18]) from 167 to 309 mm did not prevent fatal gluing. Changing  $U$  did not address the issue either. It is known that the wheel diameter has an impact on the angular velocity ( $\omega$ ) and puddle constraint; a higher diameter leads to less recirculation in the puddle, i.e., a higher cooling rate [19]. However, several wheel diameters (277, 325, and 400 mm) were trialed, and wheel diameter was not found to affect the gluing. Moreover, two copper grades were utilized, EN Cu-HCP-2.0070 and EN Cu-OF-2.0040, with thermal conductivities of  $>385$  and  $>394 \text{ W/mK}$ , respectively; however, no improvement was noticed. The  $T$  and plateau duration were varied from 1000 to 1300  $^{\circ}\text{C}$  and from 30 to 420 s, respectively. Several heating ramps were also experimented with, but no favorable outcome was obtained. The frequency of the induction heating generator (True-Heat 7030 MF TRUMPF) was switched from 39.2 to 18.9 kHz to alter the depth penetration of the electromagnetic field in the melt. Indeed, it has been reported that electromagnetic vibrations can influence crystal nucleation in bulk metallic glasses [20]. Two casts were produced at 1000 and at 1200  $^{\circ}\text{C}$ , with a power of 25 kW for the ramp and 5.6 kW for the plateau (maximum 33 kW); both casts exhibited gluing. In comparison, for MS1, the frequency of the induction heating generator was 9.3 kHz. As observed in Fig. 2b, MS2 had 2.43 m of collecting tube for the ribbon. As displayed in the previously mentioned video [14], a gas knife helps the ribbon



Fig. 3 – Example of a glued ribbon.

to overcome adhesive forces and depart from the wheel. By altering the He flow, the position where the ribbon hits the tube was changed from being close to the wheel to being at the tube end. Neither position affected the gluing phenomenon, however. Chemical analyses of the ribbon surface produced by MS1 and MS2 was carried using X-ray photoelectron spectroscopy (XPS) [21] and no difference was noticed. Moreover, for MS1 and MS2, the wheel and nozzle vibrations, measured using a laser Doppler vibrometer (Polytec OFV 303), exhibited no significant differences. Nonetheless, in the following section, we present two main parameters affecting the gluing phenomenon.

### 3.1.1. Applied pressure slope and value

The nozzle geometry is a key factor influencing  $\Delta P$ . The reported  $\Delta P$  is the difference between the applied pressure and the measured chamber pressure. Here, we do not consider the change in the hydrostatic pressure. The hydrostatic pressure due to gravity was calculated to be 27.5 mbar. To recall, our process was developed with MS1, without pressure compensation. This resulted in a loss of pressure during casting. Even when  $\Delta P$  was controlled using one buffer tank (Fig. 2b), the pressure decreased during the casting process. The nozzle geometry is presented in Fig. 4. The crucible consists of two pieces, an upper part and a lower part, which have a constant wall thickness and are screwed together. The crucible material needs to be highly heat-resistant, have good heat conduction, and be non-metallic. High-density graphite (FE-379, Schunk) was used for our Ti–Zr–Ni alloy. A metallic lid was used to close the crucible. To monitor  $\Delta P$ , the upper part of the crucible was equipped with a pipe connected to a pressure gauge. Unexpectedly, the shape of the lid was found to affect  $\Delta P$  for MS2. For a cylindrical lid shape, the  $\Delta P$  slope was more pronounced in comparison with that for a cone-shaped lid. To investigate this aspect, we tested the shape of the lid on MS1. Figure 4 shows  $\Delta P$  plotted for two applied pressures. Even when the pressure value was lower, a more horizontal slope led to the production of a glued ribbon for MS1. As MS1 was

always equipped with a cylindrical lid, this effect was not observed. From Bernoulli's momentum balance equation, assuming that the melt is an incompressible fluid and in a stationary state, for the PFC process,  $\tau \approx U^{-1}$  and  $\tau \approx \Delta P^{0.5}$  [22]. This implies that decreasing  $U$  affects the puddle region more than decreasing the pressure does.

As seen in Fig. 4, the applied pressure was not constant during the cast. To compare pressure values, the start and end values of a linear fit of the applied pressure were determined. These pressure values are plotted in Fig. 5 for MS1 and MS2, for nozzles with both a cylindrical and a conical shape. For MS1 (ribbons 61–84) and for starting a  $\Delta P$  above 230 mbar, the ribbons were systematically glued, with the exception of ribbon 73. For this cast, the nozzle lid was conical, leading to a flat  $\Delta P$  slope (blue curve in Fig. 4). This trend was observed in the case of MS2 as well, and the ribbons were glued even for really low  $\Delta P$  values. Even if some parameters were not constant for the casts presented in Fig. 5, it can be established that the angular velocity,  $\omega$ , did not have a detrimental effect on the gluing. For MS1,  $\tau$  was in the range of 34–55  $\mu\text{m}$ ; for MS2,  $\tau$  was in the range of 33–50  $\mu\text{m}$ .

### 3.1.2. Nozzle inclination

The investigations concerning the parameters presented in Fig. 1 were not solving the gluing of the ribbon, leading to the hypothesis that geometrical aspects were involved, such as the position or angle of the nozzle relative to the wheel. Madireddi et al. posited that the crucible inclination influences the ribbon thickness; they used a numerical model to examine the effect of clockwise (CW) and counter-clockwise (CCW) inclination of the crucible on puddle formation [23]. Here, the angle,  $\theta$ , is defined as the one between the vertical axis and the nozzle inclination, and the direction of the wheel rotation is CW (right for Fig. 1). Keeping all parameters constant ( $G = 0.28$  mm,  $\Delta P = 200$  mbar,  $U = 19.7$  m/s, and  $T = 1125$  C),  $\theta$  was varied for the CW and CCW directions, and  $\tau$  was measured (Fig. 6a). Similar to the findings of Madireddi et al. [23],  $\tau$  increased for both directions. For the numerical

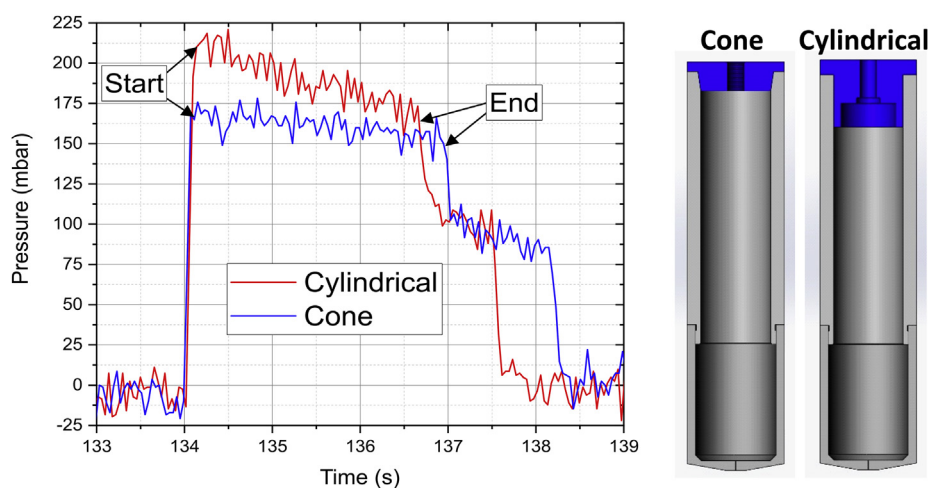


**Fig. 4** – Pressure during casting for MS1 with a cone-shaped or cylindrical lid. The crucibles with cone-shaped and cylindrical lids are displayed on the right.

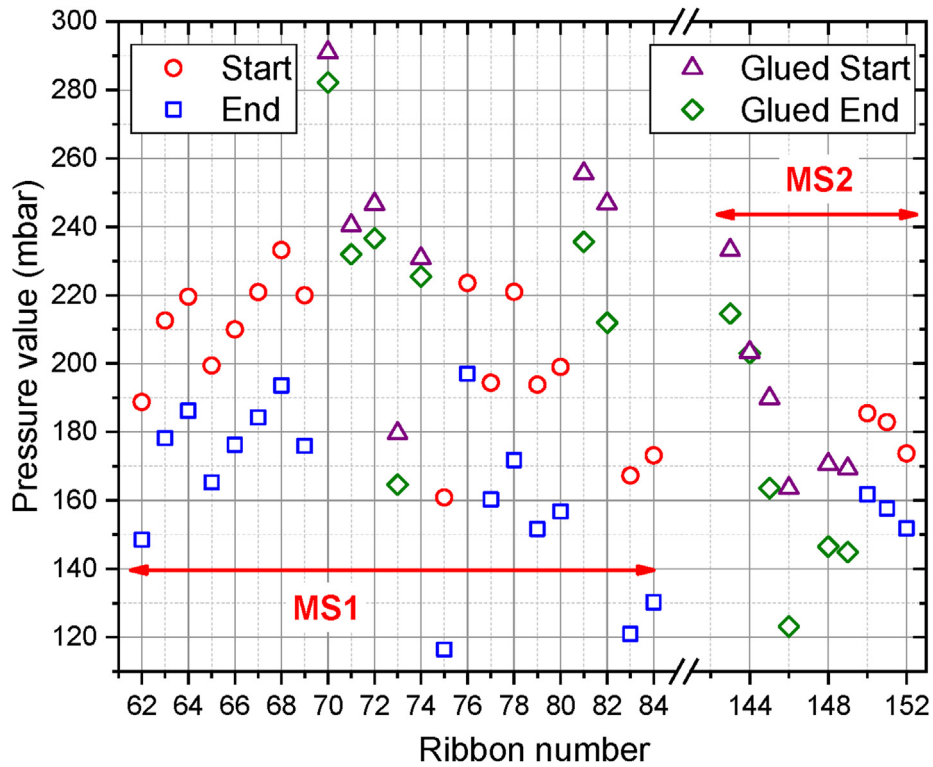


**Fig. 5** –  $\Delta P$  at the start and end of casting for MS1 (61–84) and MS2 (143–152). For the glued ribbons, values are displayed with purple triangles and olive diamonds. Successful casts are displayed with red circles and blue squares.

simulation performed by Madireddi et al., cavities were produced in the puddle for  $\theta > 2.7^\circ$  under CW inclination, and for  $\theta > 3.2^\circ$  under CCW inclination. The cavities degraded the ribbon quality, leading to a striated ribbon. In this study, striated ribbons started to appear at approximately  $\theta = 3.5^\circ$  under CW inclination and at  $\theta = 7^\circ$  under CCW inclination. Figure 6c) and 6d) shows ribbon images for  $\theta = 3.5^\circ$  under CW and CCW inclination, which depict the striation. For the experiment with  $\theta = 3.5^\circ$  under CCW inclination (Fig. 6d), an HB pattern was formed, which was not the case for  $\theta = 0^\circ$  (Fig. 6b). Interestingly,  $\tau$  was larger for the CW direction, which is in

contrast to the findings of Madireddi et al. [23]. This is most likely due to the striated ribbon, which results in over-estimation of the ribbon thickness measured using a digital micrometer. To explore ribbon gluing further, the relationship between nozzle inclination and sticking was analyzed, as described in the next section.

3.1.3. Summary of ribbon gluing

In summary, analyses of the applied pressure, linear and angular velocity, cast temperature, wheel copper grade, induction heating generator frequency, and ribbon impact

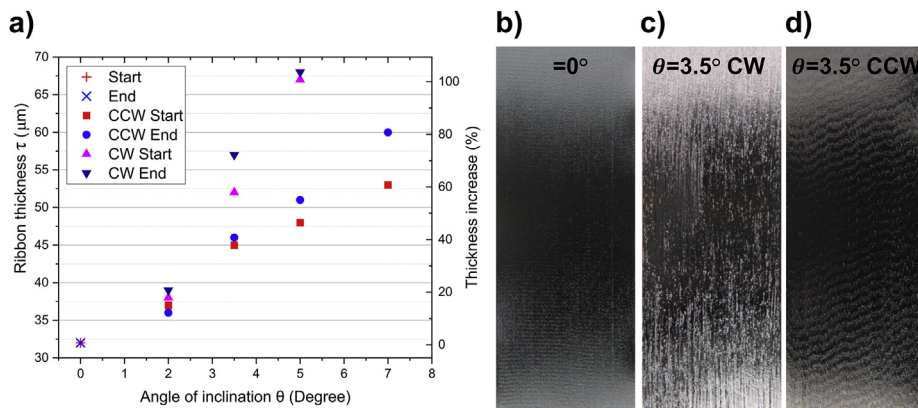


**Fig. 6** –  $\tau$  as function of  $\theta$  for CW and CCW directions. The thickness is given at the start and end of the ribbon length. Photographs of ribbons for  $\theta = 0^\circ$ ,  $3.5^\circ$  CCW, and  $3.5^\circ$  CW (width,  $W = 35$  mm).

position revealed that neither factor affected the gluing phenomenon. The actual measurement of  $\Delta P$  was found to be a crucial parameter for understanding that the  $\Delta P$  slope during the casting process was an important metric. One of the main factors was the nozzle inclination, which was not  $0^\circ$  at the beginning for MS2, but was approximately  $4^\circ$  CW. Another discrepancy between MS1 and MS2 was  $G$ . For both melt spinners,  $G$  was set in the same manner. However, due to the different motions of the mechanical components in MS2, the real  $G$  value was lower than expected. This was compensated for later on by a larger  $G$  value. By adjusting the last three variables, it was possible to mitigate the gluing phenomenon considerably. Indeed, the aforementioned parameters were found to have a direct influence on the puddle and the recirculation in the puddle, and subsequently, on the ribbon cooling rate. Numerical simulations of fluid flow and heat transfer in the PFC process have revealed that an increase in the gap distance from 0.2 to 0.4 mm would cause a slow solid/liquid interface growth, indicating a lower cooling rate for a larger gap distance [19,24]. Moreover, for  $\theta > 0^\circ$ ,  $\tau$  was shown to increase (Section 3.1.2), resulting in increments in the puddle size and puddle recirculation and leading to a lower cooling rate [23]. Furthermore, for a conical nozzle lid, i.e., a horizontal  $\Delta P$  slope (Fig. 4), with the RBR, the puddle expanded, and the puddle recirculation increased, thus lowering the cooling rate. All the investigations presented herein appeared to validate the reported numerical simulation results and appeared to clarify the relationships between the puddle length, puddle recirculation, and cooling rate.

### 3.2. Controlling ribbon thickness using Reimann Brake Ramp

As explained in Section 2.2, the RBR can be used to control the ribbon thickness. Figure 7a shows  $\tau$  at the end of the ribbon

( $>35$  m). In this diagram, the casting parameters are constant for all ribbons ( $U = 19.7$  m/s), and the thickness at the start is  $34 \mu\text{m}$ . Using the RBR, it was possible to control  $\tau$  as a function of the ribbon length. Figure 7b shows  $\tau$  at the start and end of each ribbon, with the values being obtained by applying the RBR at 360 rounds per minute (rpm), i.e. breaking the wheel at the start of the cast by 360 rpm. The ribbon thicknesses were  $40\text{--}50 \mu\text{m}$ . For this case, the maximum percentage of ribbon thickness variation was around a few percent. In Fig. 7b is also plotted  $\tau$  for the ribbons without the RBR i.e., for a constant velocity. The thickness value was more than  $8 \mu\text{m}$  lower at the end compared to the start. This is around 20% thickness variation in comparison to a few percent using the RBR.

In addition, the steady flow in the puddle region is predominantly inviscid and can be modeled analytically by combining mass and Bernoulli balances. If a certain solidification rate (typically  $>10^6$  K/s) was achieved, the thermal variables of viscosity and surface tension did not play significant roles in determining  $\tau$ . The flow dynamic equilibrium was mainly balanced between the pressure and the initial force. Assuming that molten metal is an ideal incompressible fluid, the flow rate leaving the nozzle is given as  $u_{in} = (2\Delta P/\rho)^{1/2}$ , where  $\rho$  is the density. From mass conservation, the gap-averaged flow velocity within the puddle,  $\bar{u}$ , is given by  $Bu_{in} = G\bar{u}$  and with the continuity equation  $Bu_{in} = \tau U = G\bar{u}$ . As reported by Carpenter et al. [25], combining these results gives the dimensionless scaling with the following form:

$$\frac{\tau}{G} = a \left( \frac{\Delta P}{\rho U^2} \right)^b \tag{1}$$

where  $\rho$  is the alloy density, and the coefficient  $a$  and the exponent  $b$  are determined for one set of  $B/G$ . Least-squares analysis was performed to determine the unknown constants  $a$  and  $b$ . Figure 8 shows the variation in the dimensionless thickness parameter  $\tau/G$  with the Euler number ( $Eu =$

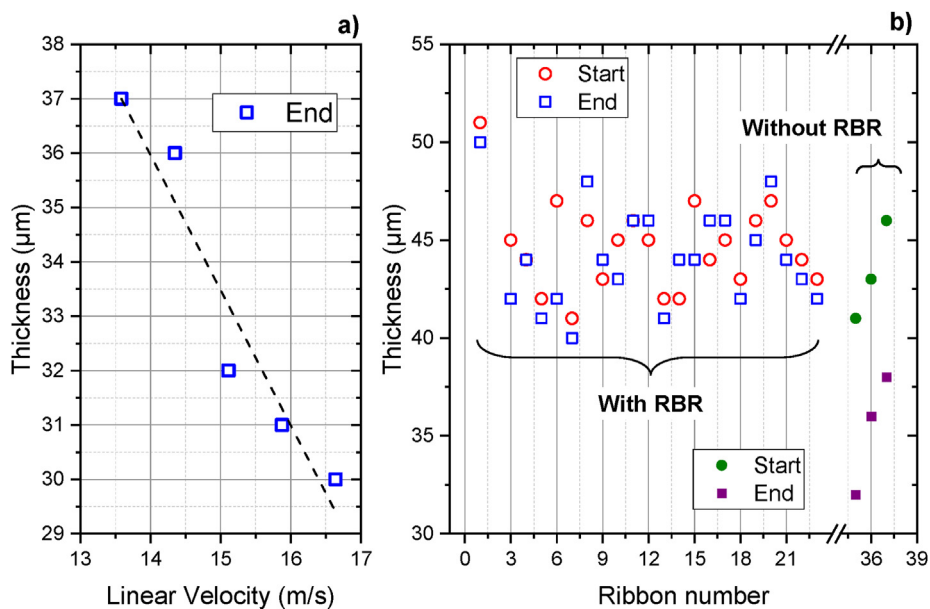
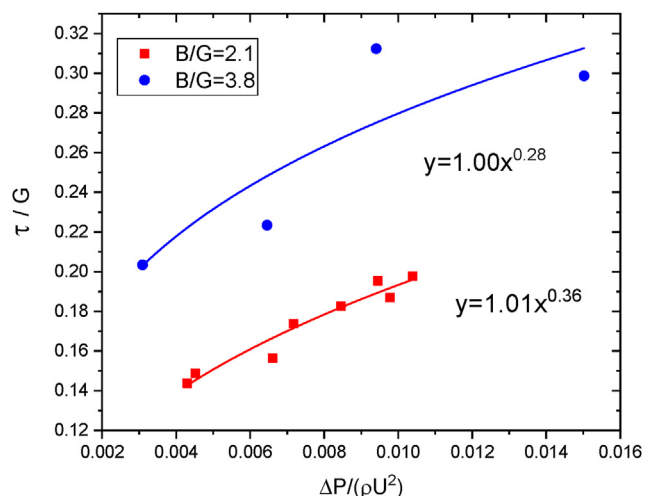


Fig. 7 – a) Ribbon thickness measured at the end of the ribbon as a function of linear velocity. b) Thickness measured at the start and end of the ribbon for several tests.



**Fig. 8** – MS1 trends of  $\tau/G$  versus  $\Delta P/\rho U^2$  with fixed  $B/G$  values.

$\Delta P/\rho U^2$ ) at assigned values of  $B/G$  for the Ti–Zr–Ni alloy used in this study. This relationship follows an allometric scaling with an exponent value close to the theoretical value of  $1/3$  [15,26,27]. It is evident that  $\tau$  increased with increasing pressure difference and decreased with increasing wheel speed. An increasing breadth ( $B/G$ ) led to an increase in the thickness ( $\tau/G$ ). This was expected, because for a fixed pressure drop, a larger entrance channel would favor a higher mass flow rate.

### 3.3. Herringbone formation on metallic glass ribbon

As has been extensively reported for crystalline ribbons, the puddle holding the melt is subjected to motion, which can lead to thickness variations that appear as casting lines or marks spanning the ribbon width. Two types of defects appear on the ribbon due to meniscus vibrations; these are called crosswave and HB [28]. HB lines are similar to cross wave lines but have shorter wavelengths. Cox et al. reported that a pinned USM was correlated with HB and that an unpinned USM was correlated with cross wave. More recently, three-dimensional (3D) numerical simulations have revealed that the pinning of the USM to the nozzle slit leads to continuous air ingress, which is in agreement with experimental observations [29]. The air entering the puddle acts as an insulator reducing the heat transfer from the puddle to the wheel, thus causing a reduction in ribbon thickness. The HB defect may therefore occur due to the presence of an air pocket on the wheel side. Due to the pinning, there was no recirculation of the molten metal in the puddle region in this study. One study reported the occurrence of HB defects for an amorphous ribbon and attributed the finding to the highest applied wheel speed [30]. For one of the experiments presented herein,  $G$  was changed from 0.25 to 0.4 mm, leading to an increase in  $\tau$  from 46 to 60  $\mu\text{m}$  and resulting in HB defect formation along the entire ribbon. This is in line with the unpinning of the meniscus at higher  $G$  values. Recently, Liu et al. reported that an increase of  $G$  reduced the size of the melt puddle [19].

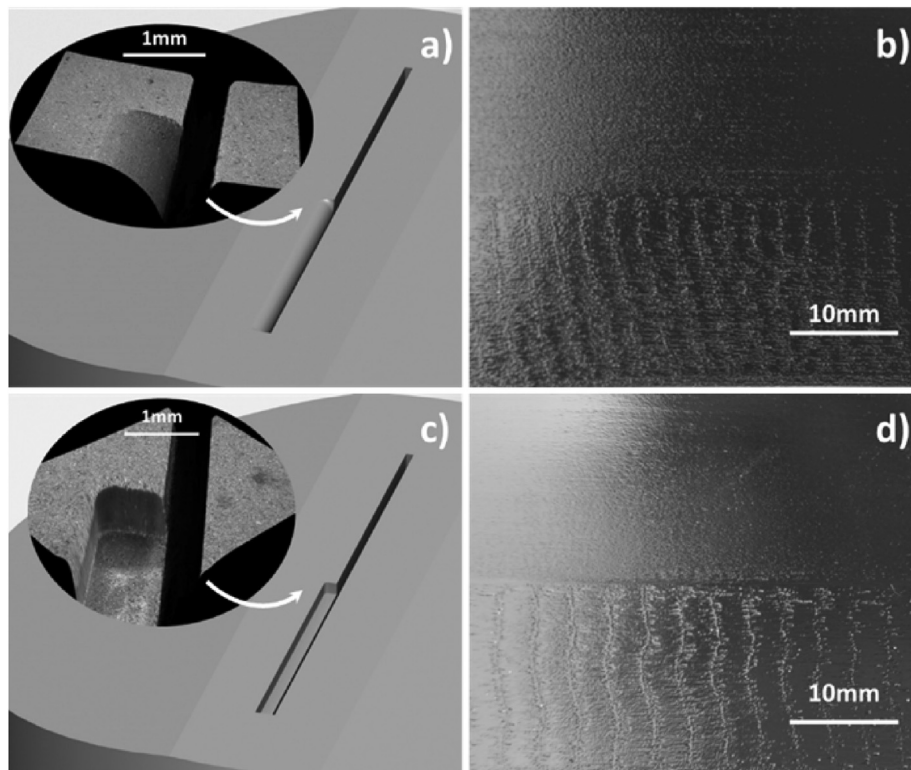


**Fig. 9** – Computer-aided design model of the nozzle. Half of the nozzle had a standard square corner (top) and the other half a purposely rounded (a) and squared (c) corner. The images of the rounded ( $R = 0.8$  mm) and squared ( $D = 0.8$  mm) corners are displayed in the enlarged areas. Photographs of ribbons produced by the rounded (b) and squared (d) step-change nozzles.

Another aspect that may play a role in HB defect formation is the wheel roughness. Su et al. reported that the occurrence of HB defects increased when the wheel roughness decreased from 1.39 to 0.12  $\mu\text{m}$  [31]. They posited that a smoother wheel surface is wetted more easily by the molten metal. As a result, the USM moves closer to the nozzle and becomes pinned at the nozzle edge. In the present study, an experiment was conducted by reducing the wheel roughness from 0.2 to 0.07  $\mu\text{m}$ , which led to HB defect formation along the entire length (not the case for  $R_a = 0.2 \mu\text{m}$ ). As stated before, with 420 g of alloy per cast, the length of ribbon produced varied from 30 to 100 m. At the longest scale, if the shrinking of  $G$ , reduction in applied pressure, wheel expansion, etc. are not adequately compensated for, the flowrate will decrease, i.e., the puddle will tend to pin, and HB defects will be formed. This was often observed for casts at the end of the ribbon. Reducing  $U$ , i.e., adjusting the RBR, addressed this issue.

To further investigate the cause of HB defects, customized nozzles that enabled the formation of HB defects were devised. Figure 9 shows a computer-aided design model of the nozzle. Half of the nozzle had a standard square corner (top), and the other half had a custom-designed rounded corner (Fig. 9a, bottom). An image of the rounded ( $R = 0.8 \text{ mm}$ ) corner, captured using a digital microscope, is displayed in the enlarged area. The helium side of the ribbon (Fig. 9b) produced by the step-change nozzle resulted in HB defect formation at the rounded side (bottom). The distance between the periodic casting lines, with an average wavelength  $\lambda$ , was manually calculated and was determined to be approximately 2.5 mm. For another experiment, a rounded corner with  $R = 0.3 \text{ mm}$  was used. Casting with this nozzle resulted in no HB formation. In the final experiment, a rectangular section of the upstream edge was removed across a half-length of the slot, producing an L-shaped notch in the inlet nozzle. A photograph of the nozzle with a notch of  $0.8 \text{ mm} \times 0.8 \text{ mm}$  is shown in Fig. 9c). HB defects were seen in the notched part (Fig. 9d). The results of these experiments are in agreement with the explanation provided by Cox et al. [28], i.e., a pinned USM is necessary for the formation of HB. For the sharp corner (unmodified), the meniscus was unpinned, whereas for the rounded or notched corner, the USM was pinned. For a rounded corner with  $R = 0.3 \text{ mm}$ , the USM was at a sufficient distance from the edge and was not pinned; hence, no HB defects were formed.

#### 4. Conclusion

A new automatized melt spinner was developed to manufacture amorphous ribbons using planar flow casting. Monitoring and controlling the process parameters was crucial to understanding the gluing phenomenon that occurred during the initial phase. The pressure applied to the melt, the nozzle inclination, and the distance between the nozzle and wheel were found to be the key parameters affecting the ribbon cooling rate. This was related to the puddle geometry and the recirculation in the puddle, both of which lowered the ribbon cooling rate. Furthermore, through a reduction in the wheel speed at the start of the casting, using the RBR, a uniform

thickness was successfully achieved along ribbons with lengths of over 50 m. A  $7^\circ$  CCW nozzle inclination was found to increase the ribbon thickness by 80%, while the ribbon quality started to be degraded under a  $3.5^\circ$  CW rotation. An allometric scaling with an exponent value close the theoretical value of  $1/3$  could describe the variation in the dimensionless thickness parameter,  $\tau/G$ , with the Euler number ( $Eu = \Delta P/\rho U^2$ ) at assigned values of  $B/G$ . Moreover, customized nozzles that enabled the formation of HB defects were devised. These defects were found to be directly correlated with the pinning of the liquid puddle at the nozzle edge.

On the engineering level, our observations suggest possible tools for achieving high quality ribbons with control thickness over a large length. Further studies with different  $B/G$  values will be helpful to extend our allometric scaling validity.

#### Dedication

This work is dedicated to the memory of Dr. h.c. Peter Reimann who passed away in November of 2021. At the end of the 1970s, for the start of the planar flow casting at the University of Basel, he developed the Reimann Brake Ramp to produce high-quality ribbons with controlled thickness over a considerable length. Always involved in metallic glasses, in 2017 he initiated the construction and realization of the new Melt Spinner 2. He was an enthusiastic researcher and excellent communicator, and during his career he not only contributed to the scientific successes of the department, but also shared the fascination of the natural sciences with a broad audience at public events. He is sorely missed.

#### Declaration of Competing Interest

The authors declare that they have no known competing financial interests or personal relationships that could have appeared to influence the work reported in this paper.

#### Acknowledgments

The authors would like to thank the electronic and mechanical workshops from the Department of Physics of the University of Basel for their contributions towards helping to construct MS1 and MS2. We would like to warmly thank Paul Steen<sup>†</sup> from the Robert Frederick Smith School of Chemical and Biomolecular Engineering, Cornell University, USA, for his helpful discussion during this three year process.

#### REFERENCES

- [1] Zou J, Jiang Z, Zhao Q, Chen Z. *Mater Sci Eng, A* 2009;507:155–60.
- [2] Zhang F, Wu J, Jiang W, Hu Q, Zhang B. *ACS Appl Mater Interfaces* 2017;9:31340–4.
- [3] Kong X, Yang Y, Guo S, Li R, Feng B, Jiang D, et al. *J Mater Sci Technol* 2021;71:163–8.

- [4] Zhang Y, Zhai T, Li B, Ren H, Bu W, Zhao D. *J Mater Sci Technol* 2014;30:1020–6.
- [5] Phair JW, Gibson MA, Basile A. In: Gallucci F, editor. *Membr. Membr. React.* Chichester, UK: John Wiley & Sons; 2011. p. 435–57.
- [6] Sundararajan A, Thomas B. *TMS Light Met* 2008:793–809.
- [7] Theisen EA, Weinstein SJ. *ArXiv: 2104.09251 cond-mat*. 2021.
- [8] Ma D, Wang Y, Li Y, Umetsu RY, Ou S, Yubuta K, et al. *J Mater Sci Technol* 2020;36:128–33.
- [9] Rohr L, Reimann P, Richmond T, Güntherodt H-J. In: *Rapidly quenched mater.* Elsevier; 1991. p. 715–7.
- [10] Pawlak R, Marot L, Sadeghi A, Kawai S, Glatzel T, Reimann P, et al. *Sci Rep* 2015;5:13143. <https://doi.org/10.1038/srep13143>.
- [11] Shirzadi AA, Koziele T, Cios G, Bala P. *J Mater Process Technol* 2019;264:377–81.
- [12] Zheng Y, Xie H, Zhang Q, Suwardi A, Cheng X, Zhang Y, et al. *ACS Appl Mater Interfaces* 2020;12:36186–95.
- [13] Byrne CJ, Theisen EA, Steen PH, Reed BL. *Metall Mater Trans B* 2006;37:445–56.
- [14] Reimann P, Breitenstein H, Jakob S, Martina M, Marot L, Mattson J, et al. In: 71th annu. Meet. APS div. Fluid dyn. - gallery fluid motion. Atlanta, GA: American Physical Society; 2018. <https://doi.org/10.1103/APS.DFD.2018.GFM.V0053>.
- [15] Su Y-G, Chen F, Chang C-M, Wu C-Y, Chang M-H, Chung CA. *J Occup Med* 2014;66:1277–86.
- [16] Li Y, Yang Y, He C. *J Non-Cryst Solids* 2018;481:276–81.
- [17] Sowjanya M, Kishen Kumar Reddy T. *J Mater Process Technol* 2014;214:1861–70.
- [18] Liebermann HH. *Metall Trans B* 1984;15:155–61.
- [19] Liu H, Chen W, Qiu S, Liu G. *Metall Mater Trans B* 2009;40:411–29.
- [20] Tamura T, Amiya K, Rachmat RS, Mizutani Y, Miwa K. *Nat Mater* 2005;4:289–92.
- [21] Iyyakkunnel S, Marot L, Eren B, Steiner R, Moser L, Mathys D, et al. *ACS Appl Mater Interfaces* 2014;6:11609–16.
- [22] Fiedler H, Muehlbach H, Stephani G. *J Mater Sci* 1984;19:3229–35.
- [23] Madireddi S. *Int. J. Comput. Phys. Ser.* 2018;1:279–85.
- [24] Wu SL, Chen CW, Hwang WS, Yang CC. *Appl Math Model* 1992;16:394–403.
- [25] Carpenter JK, Steen PH. *Int J Heat Mass Tran* 1997;40:1993–2007.
- [26] Carpenter JK, Steen PH. *J Mater Sci* 1992;27:215–25.
- [27] Praisner TJ, Chen JSJ, Tseng AA. *Metall Mater Trans B* 1995;26:1199–208.
- [28] Cox BL, Steen PH. *J Mater Process Technol* 2013;213:1743–52.
- [29] Swaroopa M, Reddy TKK, Reddy AC, Majumdar B, 7 (2016) 6.
- [30] Sohrabi S, Arabi H, Beitollahi A, Gholamipour R. *J Mater Eng Perform* 2013;22:2185–90. <https://doi.org/10.1016/j.matpr.2017.02.135>.
- [31] Su Y-G, Chen F, Wu C-Y, Chang M-H. *J Mater Process Technol* 2016;229:609–13.